ACS OMEGA

Open Access

http://pubs.acs.org/journal/acsodf

Article

Investigation on Adsorption Pore and Fractal Analyses of Low-Rank Coals in the Northern Qaidam Basin

Xuejiao Zhou, Qian He, and Haihai Hou*

Cite This: *ACS Omega* 2024, 9, 9823−9834

Read Online

ACCESS | Metrics & More | Article Recommendations

ABSTRACT: The northern Qaidam Basin has abundant coal and coalbed methane (CBM) resources, and quantitative evaluation of adsorption pore characteristics has great significance for optimum selection of CBM-favorable areas. Based on vitrinite reflectance, coal maceral, proximate analysis, low-temperature N_2 adsorption, and methane isothermal adsorption experiments, the heterogeneities of adsorption pores (pore diameter <100 nm) were quantitatively characterized, and relationships between fractal dimensions and physical parameters of low-ranked coal reservoirs were revealed. The results show that the micropore volume percentage ranges between 33.70 and 86.44% with an average of 64.94%. Based on N_2 adsorption/desorption curves and pore diameter distribution characteristics, the adsorption pore structures of low-ranked coals were divided into 3 types. According to the FHH model, fractal dimension D_1 (relative pressure between 0 and 0.5) and D_2 (relative pressure between 0.5 and 1) were calculated. Fractal dimension D_1, representing adsorption pore surface area, ranges from 2.001 to 2.345, with lower values. Fractal dimension D_2 (adsorption pore structure) is from 2.641 to 2.917, with relatively high values, which has a decreasing tendency from west to east in the study area. There are positive relationships between fractal dimension D_1 and Langmuir volume and specific surface area, whereas negative correlations are found between fractal dimension D_2 and Langmuir pressure, ash yield, moisture content, volatile content, and average pore diameter. Combined with the related data for middle- and high-rank coals, the characteristics of pore surface and methane adsorption capacity can be analyzed based on the variation of vitrinite reflectance. Furthermore, the complexity of pore structure can also be predicted according to the averaged pore size and micropore content to some degree.

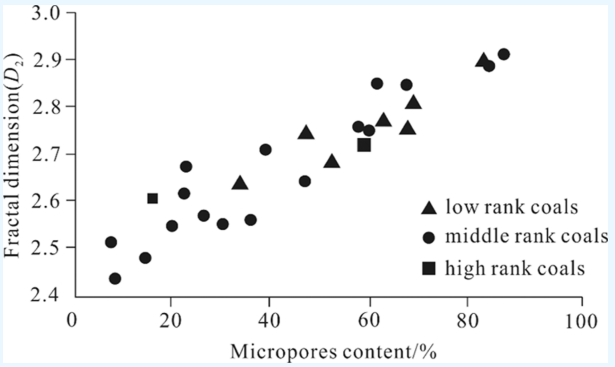

1. INTRODUCTION

As a complex porous medium with high heterogeneity and anisotropy, the system of coal pore structure affects the adsorption performance and a series of production processes, such as coalbed methane (CBM) desorption, diffusion, and seepage, which have been focused on by domestic and foreign scholars.[1−4] According to a previous study,[5] pore systems in coal reservoirs are divided into micropores (pore diameter <10 nm), transitional pores (10−100 nm), mesopores (100−10^3 nm), and macropores (>10^3 nm). Based on the influence of pores on CBM reservoir and permeability, the pore types of coals can be divided into adsorption pores less than 100 nm and seepage pores greater than 100 nm according to the pore size.[5−7] Among them, the development of adsorption pores controls the physical adsorption and desorption processes of CBM, which is closely related to the methane adsorption capacity and gas content; thus, it is very important for the evaluation of CBM exploration and coal mine gas control.

From the perspective of CBM exploration, previous studies have been focused on areas such as coal gathering characteristics, CBM resource evaluation, and CBM formation condition.[8−10] Fractal dimension has gradually become known in recent years as a quantitative parameter to characterize the heterogeneity of pore structure.[11] It has been proven that the porous media in coal reservoirs have obvious fractal characteristics at different research scales.[12−14] At present, the widely used fractal characterization methods of coal reservoir pores are based on CO_2 adsorption, low-temperature N_2 adsorption, mercury injection method, and nuclear magnetic resonance experiments.[15−17] The calculation methods include the Brunauer−Emmett−Teller (BET) model, Langmuir model, FHH model, thermodynamic model, and Menger sponge model.[18,19] However, due to the existence of high heterogeneity, several scholars have reached different

Received: January 7, 2024
Revised: February 8, 2024
Accepted: February 9, 2024
Published: February 17, 2024

https://doi.org/10.1021/acsomega.4c00211
ACS Omega 2024, 9, 9823−9834

conclusions on the classification of coal pore types and the characterization of fractal dimensions, especially the adsorption and permeability responses of fractal dimensions under different coal rank conditions.[13,14] The quantitative characterization techniques and analysis methods of pore structure in coal are mainly divided into the fluid injection method, the nonfluid injection method, and the image analysis method, including CO_2 adsorption, low-temperature N_2 adsorption, the mercury injection method, nuclear magnetic resonance, CT scanning, optical microscopy, scanning electron microscopy (SEM), transmission electron microscopy, X-ray diffraction, and atomic force microscopy.[20−22] The pore structure of coal is characterized by pore surface area, pore volume, pore distribution, average pore size, pore morphology, pore connectivity, and fractal dimension.[23,24] A part of studies usually focuses on the pore fractal characteristics within relatively narrow coal-grade ranges in the same region. However, there is little attention on whether the research results from a narrow coal-grade range are in agreement with those from a large coalification range. Furthermore, the variation of fractal dimension and its physical meaning can be analyzed indirectly through the parameter values in a large coalification range, thus avoiding the complicated process of calculating fractal dimension.

Taking the Middle Jurassic coals in the northern Qaidam Basin as the research object, this paper analyzes the characteristics of adsorption pores with low-rank coals based on a series of experiments, which reveals the physical significance of coal adsorption pores under different fractal dimensions. The internal relationships between the fractal dimension of adsorption pores and methane adsorption characteristics, coal quality, and coal pore structure are discussed in detail. On this basis, the correlations are analyzed between the fractal dimension and various parameters of the coal reservoir under different coalification degrees such as low rank, middle rank, and high rank. The research results have an important significance for the occurrence characteristics of CBM and the quantitative analysis of coal reservoir physical parameters.

2. GEOLOGICAL SETTINGS

The tectonic divisions of northern Qaidam Basin generally include the northern fault block belt in the west and the Delingha depression in the east, which is composed of multiple secondary structural belts (depressions and uplifts). The coalfields in northern Qaidam are mainly distributed in the shallow depressions in the front of Qilian Mountains. Its distribution from west to east includes Saishiteng Coalfield (Saishiteng Depression), Yuqia Coalfield (western Yuqiahongshan Depression), Quanji Coalfield (eastern Yuqiahongshan Depression), and Delingha Coalfield (Delingha Depression). The Middle Jurassic in northern Qaidam Basin consists of two main coal-bearing strata from bottom to top, namely, Dameigou Formation and Shimengou Formation, with the total thickness of coal seams ranging from 2 to 35 m. Among them, F coal in Dameigou Formation and G coal in Shimengou Formation are the targets for CBM exploration due to their large thickness and stable distribution.[25,26] The Jurassic coals in northern Qaidam Basin are mainly long-flame coals with a low metamorphic degree, and gas coals are distributed in part regions. Due to a relatively dry and hot depositional environment,[27] the macrolithotypes are mainly semibright and semidull coals.

3. SAMPLE COLLECTION AND TESTING METHODS

In this paper, 8 coal samples were collected from 4 coalfields in northern Qaidam Basin, of which 7 samples were collected from coal mines, and 1 sample was collected from a borehole (YQ-1). The coal quality parameters, including the moisture content, the ash yield, and the volatile content, were obtained based on a proximate analysis using the Chinese Standard GB/T 212-2008. Maximum vitrinite reflectance ($R_{o,max}$) measurements and maceral analyses (500 points) were performed by oil immersion in reflected optical light using a Leitz MPV-3 photometer microscope, in accordance with Chinese Standards GB/T 6948-1998 and GB/T 8899-1998, respectively. The CH_4 isothermal test was performed to obtain Langmuir volume and Langmuir pressure according to Chinese Standard GB/T 19560-2208. Before the CH_4 isothermal experiment, coal samples were crushed and sieved to sizes ranging from 0.18 mm to 0.25 mm for testing. Furthermore, an IS-100 high pressure adsorption tester was used at a temperature of 30 °C and a maximum equilibrium pressure of 10 MPa. Based on vitrinite reflectance, coal maceral, proximate analysis, and CH_4 isothermal adsorption experiment, low-temperature nitrogen adsorption was carried out for each coal sample. The nitrogen adsorption is used to obtain the specific surface area, pore volume, and pore structure distribution of adsorption pores, which were tested by the NOVA2000e specific surface area and aperture analyzer. The theoretical test range of coal pores is between 2 and 200 nm, and the theoretical test specific surface area range is from 0.1 m^2/g to 3500 m^2/g. The strong luster part of coal was selected in order to decrease the influence of coal macerals on pore structure, and the selected samples were crushed, and 5−10 g of 40−60 mesh coal was screened for testing. Based on the nitrogen adsorption data, the specific surface area can be calculated by the BET method, and the pore size distribution can be obtained by the Barrett−Joyner−Halenda (BJH) model.

4. RESULTS

4.1. Development Characteristics of Adsorption Pore.

Based on the SEM and optical microscopy observations, organic pores in the Jurassic coals are relatively developed, including gas pores, tissue pores (Figure 1a,b), and unfilled pore in fusinite or semifusinite (Figure 1c,d). It should be noted that SEM is beneficial to observe the morphology of pores and fractures, but optical microscopy is beneficial to observe the types of coal macerals.[28] However, most of these observed pores are large pores and mesopores, largely due to the limitations of magnification observation. In order to better study the pore development and structural characteristics of adsorption pores (micropores) in low-ranked coal reservoirs, low-temperature nitrogen adsorption experiments were carried out, including the results of specific surface area, total pore volume, average pore diameter, and percentage volume (Table 1).

The specific surface area of Jurassic coal samples in northern Qaidam varies greatly, ranging from 0.843 to 55.12 m^2/g, with an average value of 23.34 m^2/g (Table 1). The total pore volume ranges from 2.46 to 50.43 × 10^{-3} $mL·g^{-1}$, with an average of 25.27 × 10^{-3} $mL·g^{-1}$, which shows a positive linear correlation with specific surface area (Figure 2a), indicating that the coals with higher pore volume also have a larger specific surface area. The average pore diameter is in the range of micropores, ranging from 3.78 to 4.01 nm. Except for the

https://doi.org/10.1021/acsomega.4c00211
ACS Omega 2024, 9, 9823−9834

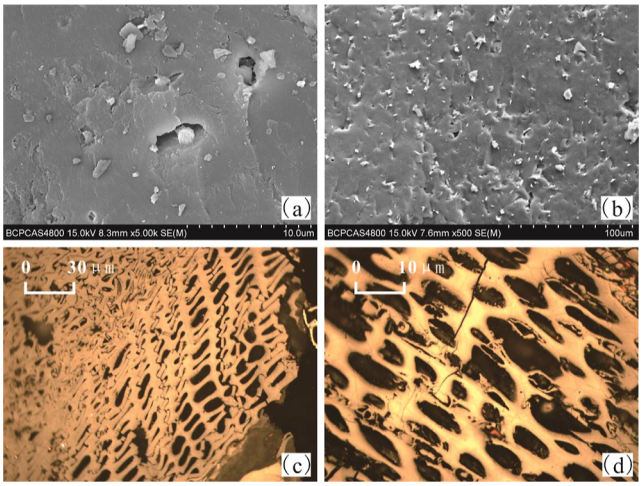

Figure 1. Observation results of SEM and photometer microscope for the Yuqia coal samples. [(a) Gas pores under SEM; (b) plant cell pores under SEM; and (c,d) cavity pores unfilled by clay in fusinite and semifusinite under optical microscopy].

coal samples from Dameigou and Lvcaogou lower layers, the percentage of micropore volume is dominant, followed by transitional pores and medium pores in a decreasing order.

The relationship between specific surface area and CH_4 adsorption capacity has been quite controversial at home and abroad.[4,29,30] For the studied samples, the relationship between the Langmuir volume and the specific surface area is not obvious (Figure 2b), which is consistent with the previous opinion showing that the correlation between the specific surface area and adsorption capacity is very weak or the correlation between them is rather complex.[31] However, there is an obvious negative correlation between specific surface area and Langmuir pressure (Figure 2c). Langmuir pressure represents the difficulty of methane adsorption by coal, and the coals with larger specific surface areas have higher adsorption rates at the initial stage (lower pressure section) and lower Langmuir pressure.

4.2. Analysis of Typical Adsorption Pore Structure Model. The experimental principle of low-temperature nitrogen adsorption conforms to the theory of pore material adsorption and condensation. Therefore, the adsorption pore morphology of coal can be identified according to the types and characteristics of coal adsorption/desorption curves. Based on the nitrogen adsorption results of coal samples in northern Qaidam Basin, the structural models of typical adsorption pores can be divided into three types: type I, type II, and type III.

Type I is represented by the F coal seam of YQ-1 well in Yuqia Coalfield. The characteristics of nitrogen adsorption/desorption curve of this type can be described as follows. The adsorption line basically rises in a two-stage pattern, with rapid rise in the early stage and stable rise in the late stage, whereas the desorption curve has an obvious hysteresis loop and presents a sharp decline stage near the relative pressure of 0.5 (Figure 3a). The pore structure represented by type I is dominated by micropores, and the pore morphology is mainly typical "ink bottle" or "fine bottleneck" shaped pores with a small mouth and a large belly. The inflection point of desorption curves of such pore structures generally occurs near the relative pressure of 0.5. The Kelvin equation is shown as follows, $r_k = \frac{-2\gamma V_L \cos\theta}{RT\ln(P/P_0)}$, where r_k is kelvin radius under the

Table 1. Experimental Results of Fundamental Tests and Low-Temperature N_2 Adsorption of the Coal Samples[a]

coal sample	coal name	$R_{o,max}$/%	proximate analysis/%			SSA/($m^2 \cdot g^{-1}$)	TPV/(10^{-3} $mL \cdot g^{-1}$)	APZ/nm	pore volume percentage/%			Langmuir volume/($m^3 \cdot t^{-1}$)	Langmuir pressure/MPa	curve type
			M	A	V				0–10 nm	10–100 nm	>100 nm			
Gaoquan	F	0.68	2.4	6.3	34.7	16.76	18.94	4.52	83.48	15.58	0.94	33.56	1.37	I
YQ-1	F	0.58	–	–	–	43.55	43.77	4.02	82.43	16.70	0.87	–	–	I
Wucai	F	0.72	2.6	2.6	27.9	55.12	50.43	3.66	86.44	13.28	0.28	32.68	0.83	I
Yuqia	F	0.51	2.0	5.4	40.9	21.3	29.48	5.53	68.21	29.55	2.24	42.19	1.20	II
Dameigou	F	0.47	7.1	14.3	40.1	2.45	6.53	10.66	33.70	57.41	8.89	36.36	1.89	III
Wanggaxiu	F	0.38	3.7	11.4	47.3	0.84	2.46	11.67	51.76	37.20	11.04	30.96	1.56	III
Lvcaogou upper layer	G	0.56	5.6	4.8	33.9	2.54	4.57	7.20	67.11	27.99	4.90	26.51	1.64	III
Lvcaogou lower layer	G	0.69	4.9	9.1	35.2	2.78	7.83	11.27	46.30	46.50	7.20	30.08	1.82	III

[a]–, no data; $R_{o,max}$, maximum vitrinite reflectance; M, moisture; A, ash yield; V, volatile; SSA, specific surface area; TPV, total pore volume; APZ, average pore diameter.

https://doi.org/10.1021/acsomega.4c00211
ACS Omega 2024, 9, 9823−9834

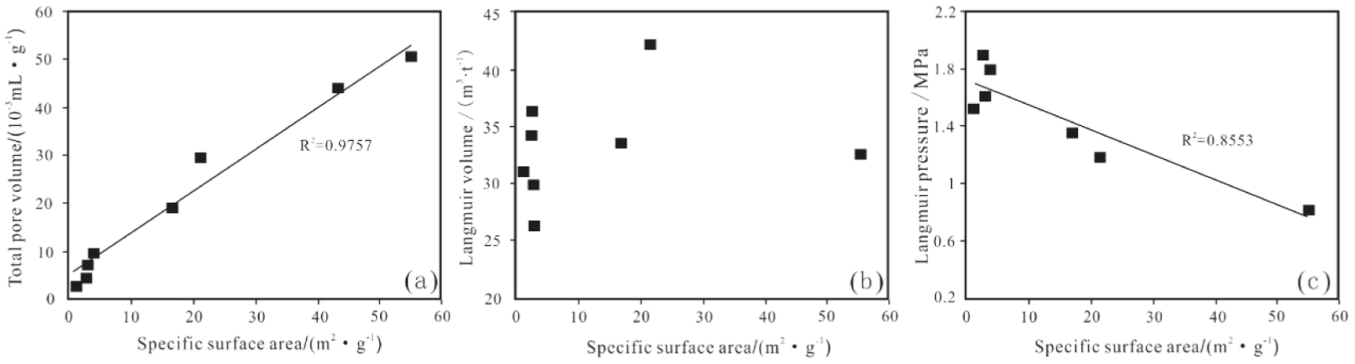

Figure 2. Relationships between total pore volume, adsorption capacity, and specific surface area. (a) Total pore volume vs specific surface area; (b) Langmuir volume vs specific surface area; (c) Langmuir pressure vs specific surface area.

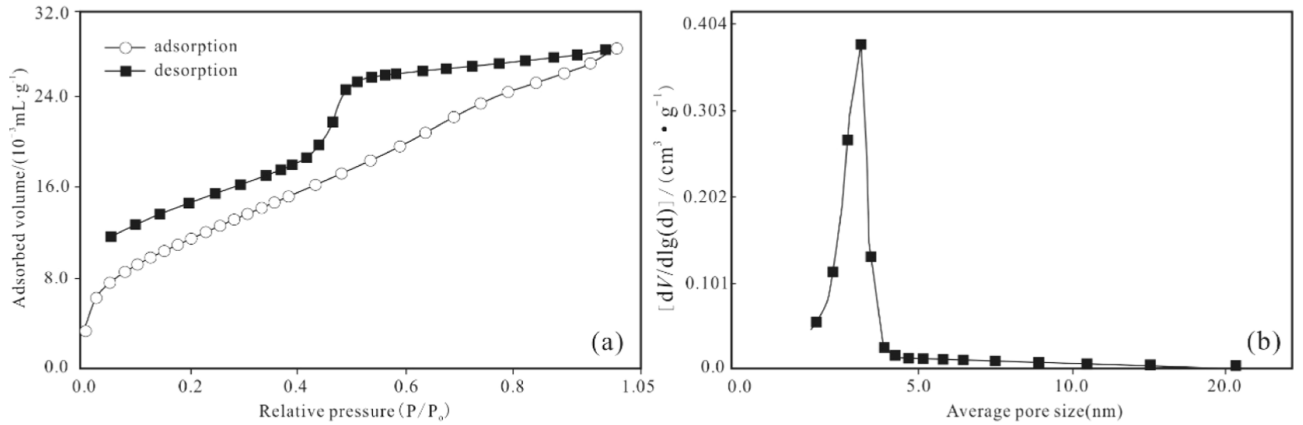

Figure 3. Characteristics of adsorption pore of type I. [(a) Adsorption/desorption curves; (b) pore diameter distribution].

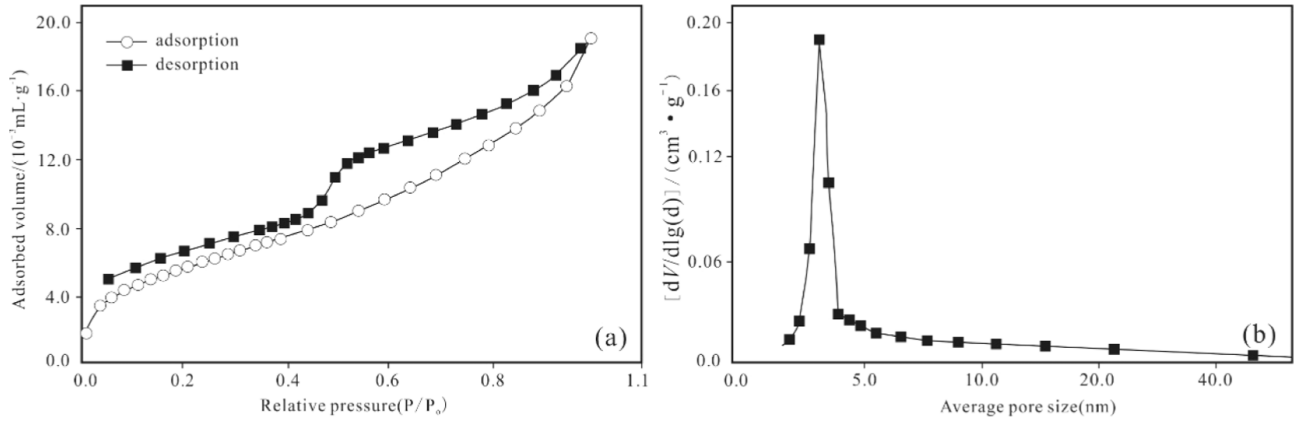

Figure 4. Characteristics of adsorption pore of type II. [(a) Adsorption/desorption curves; (b) pore diameter distribution].

relative pressure of P/P_0; γ is liquid surface tension; V_L is liquid molar volume; θ is the contact angle between liquid and pore wall; R is gas constant; and T is temperature. Kelvin radius $r_k = -2 \times 8.85 \times 10^{-3} \times 34.65 \times 10^{-4} \times 1/8.315 \times 77.3 \times \ln 0.5 = 1.38$ nm. According to the theory of Broekhoff-de Boer, the average thickness can be calculated as follows: $t = \left[\frac{A}{B - \lg\left(\frac{P}{P_0}\right)}\right]^{0.5}$, where P/P_0 is the relative pressure; A and B are the empirical values with 13.99 and 0.034, respectively. At this time, the average thickness of the adsorption layer $t = [13.99/(0.034 - \lg 0.5)]^{0.5} \times 10^{-1} = 0.65$ nm; thus, the pore radius $r_p = r_k + t = 1.38$ nm + 0.65 nm ≈ 2 nm. Finally, the aperture corresponding to the relative pressure point is obtained to be 4 nm; thus, the diameter of the bottle mouth of this "thin bottleneck" is generally about 4 nm.

The coal samples with type I curves also include Gaoquan and Wucai coal mines in northern Qaidam Basin. The specific surface area and pore volume of coal samples with such curves are relatively large. Specifically, the average specific surface area of the tested samples is 38.48 $m^2 \cdot g^{-1}$, and the average pore volume and the average pore diameter are 37.71 × 10^{-3} mL·g^{-1} and 3.8 nm, respectively. As the absolute predominance of micropores in this type of pore has a high specific surface area and volume ratio (Figure 3b; Table 1), the adsorption and storage performance of this pore type is pretty good, but it is

https://doi.org/10.1021/acsomega.4c00211
ACS Omega 2024, 9, 9823−9834

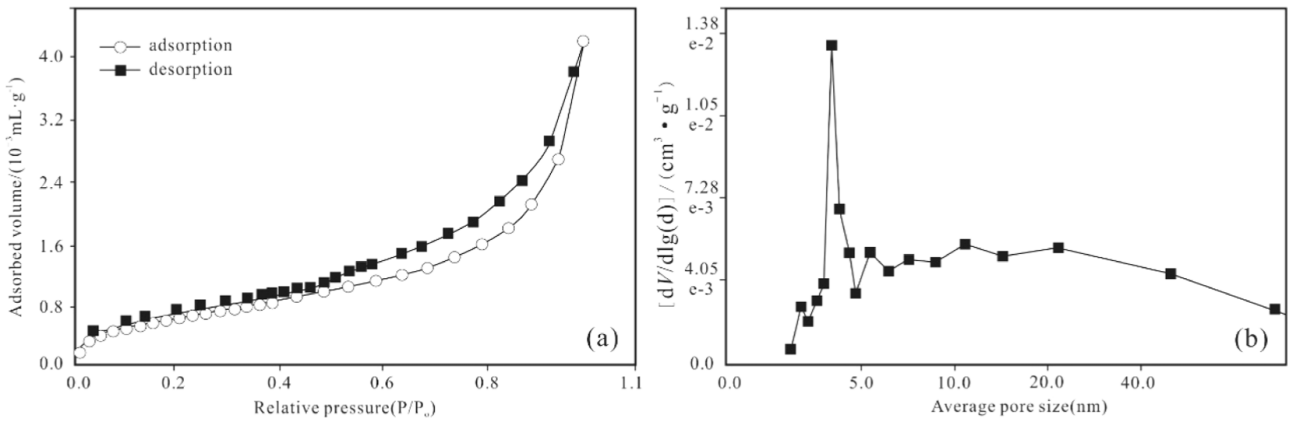

Figure 5. Characteristics of adsorption pore of type III. [(a) Adsorption/desorption curves; (b) pore diameter distribution].

relatively difficult in the desorption and diffusion stage of CBM. Furthermore, parts of the investigations show that the overwhelming peak at around 4 nm is attributed to the tensile strength effect phenomenon.[32] Thus, whether BJH desorption data can be used to analyze pore size distribution needs further discussion.

The F coal seam of Yuqia Coal Mine in northern Qaidam Basin is a typical type II. The characteristics of nitrogen adsorption and desorption curves of the samples are described as follows. The adsorption curve rises steadily, and the rising rate increases rapidly. There is an obvious hysteresis loop in the desorption curve, but the typical platform segment of type I does not appear (Figure 4a). The pore structure of type II is dominated by the development of micropores, and the pore morphology is mainly open parallel plate slit pores.[33] The relative pressure of this type of pore during condensation is higher than that during evaporation. Coal samples with type II pores can produce a hysteresis loop due to the different relative pressures during condensation and evaporation. The main difference between type II and type I is that they can produce different loop forms and have different pore structure types.

The coal samples with type II curves generally have a higher specific surface area (21.33 $m^2 \cdot g^{-1}$) and total pore volume (29.48×10^{-3} $mL \cdot g^{-1}$). The contribution of pores to surface area and total pore volume mainly comes from micropores (Figure 4b). Compared with type I pores, the transitional pore volume ratio is significantly larger (Table 1). In general, these pores are typical adsorption pores with good permeability, and thus they are favorable to the adsorption, desorption, and diffusion of CBM.

The F coals from Dachangou mine in Quanji Coalfield are a typical sample for type III (Figure 5a). The adsorption and desorption curves are basically consistent, and only a weak hysteresis loop exists. The pores represented by this type have a typical bimodal structure with high contents of both micropores and transitional pores (Figure 5b), and these pores are mainly open inclined slate-slit pores.[33] Coal samples with type III also include Wanggaxiu, Lvcaogou upper layer, and Lvcaogou lower layer. Such pores generally have low specific surface areas and low total pore volumes, with only 3 $m^2 \cdot g^{-1}$ and 8×10^{-3} $mL \cdot g^{-1}$, respectively. For the desorption and diffusion of CBM, on the one hand, the significantly increased proportion of transitional pores is conducive to the desorption of CBM; on the other hand, this bimodal pore structure may affect the gas effective diffusion.

5. DISCUSSION

5.1. Fractal Dimension Calculation of Coal Adsorption Pore. The fractal dimension of the coal adsorption pore can be calculated according to the relative pressure and adsorption capacity data. The calculation methods mainly include the fractal BET model, fractal Langmuir model, fractal FHH model, and thermodynamic model.[34,35] Among them, the FHH model method is a better calculation method, which is widely used. According to the principle of the FHH model, fractal dimension of a coal adsorption pore is calculated using the following equation

$$\ln\left(\frac{V}{V_0}\right) = \alpha + A\left[\ln\left(\ln\left(\frac{P_0}{P}\right)\right)\right] \quad (1)$$

where V is the volume of adsorbed gas molecules under the equilibrium pressure P; V_0 is the volume of adsorbed gas in the monolayer. P_0 is the saturated vapor pressure of gas adsorption; A depends on the fractal dimension D and adsorption mechanism; and α is a constant. A can be obtained by the slope of the logarithmic linear relationship between the adsorption volume and the reciprocal of the relative pressure. After A is obtained, the fractal dimension of the coal adsorption pore can be further calculated. It is worth noting that when D value is calculated by A value, different scholars have proposed two different calculation methods based on different adsorption theories,[36,37] which are $A = (D - 3)/3$ and $A = D - 3$.

The adsorption and desorption curves of coal samples have hysteresis around the relative pressure of 0.5, which reflects that there are great differences in the size and morphology of the pores before and after this relative pressure. Therefore, the relative pressure of 0.5 is taken as the calculating boundary. The above two fractal dimension equations were used to calculate the fractal dimension of the relative pressure between 0−0.5 and 0.5−1. Between the two relative pressure segments, the double logarithmic curve presents different slopes, and the fit degree between them is high (Figure 6), indicating that there are indeed two different pore fractal dimensions in the two relative pressure segments, namely D_1 and D_2. It can be seen that the fractal dimensions calculated by the equation $A = D - 3$ are in the range of 2−3, whereas the results calculated by the equation $A = (D - 3)/3$ are obviously smaller, some of which are lower than 2 (Table 2). Since the fractal dimension of the pore surface or pore structure is generally 2−3, otherwise the fractal significance of the fractal pore system will

https://doi.org/10.1021/acsomega.4c00211
ACS Omega 2024, 9, 9823−9834

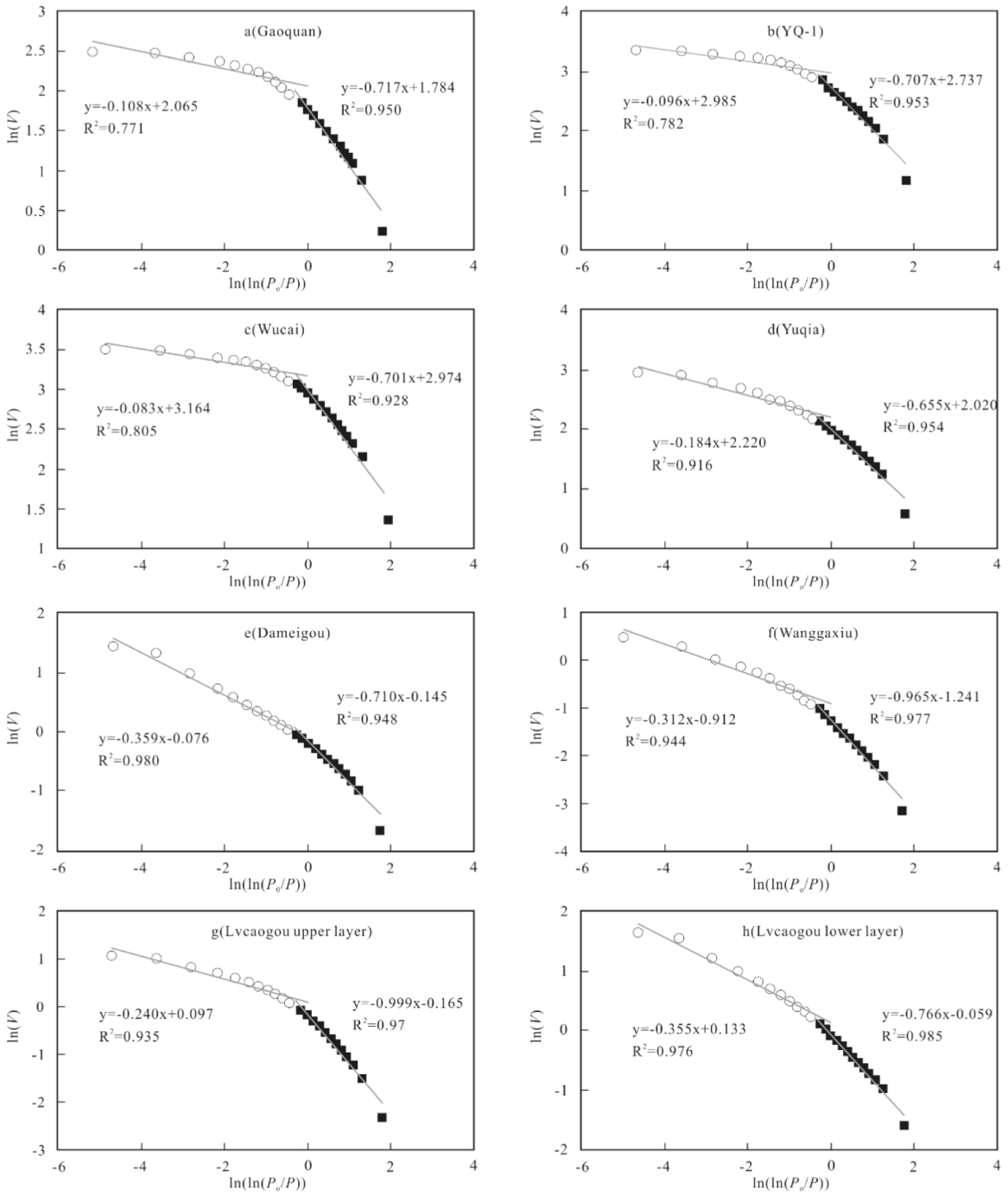

Figure 6. Double logarithmic curves between adsorption volumes and related pressures. (a) Gaoquan; (b) YQ-1; (c) Wucai; (d) Yuqia; (e) Dameigou; (f) Wanggaxiu; (g) Lvcaogou upper layer; (h) Lvcaogou lower layer.

Table 2. Adsorption Pore Fractal Dimensions Based on FHH Model of Coal Samples

coal sample	relative pressure: 0−0.5				relative pressure: 0.5−1			
	A_1	$D_1 = 3 + A_1$	$D_1 = 3 + 3A_1$	R_1^2	A_2	$D_2 = 3 + A_2$	$D_2 = 3 + 3A_2$	R_2^2
Gaoquan	−0.717	2.283	0.849	0.95	−0.108	2.892	2.676	0.77
YQ-1	−0.707	2.293	0.879	0.95	−0.096	2.904	2.712	0.78
Wucai	−0.701	2.299	0.897	0.93	−0.083	2.917	2.751	0.81
Yuqia	−0.655	2.345	1.035	0.95	−0.184	2.816	2.448	0.92
Dameigou	−0.71	2.290	0.87	0.95	−0.359	2.641	1.923	0.98
Wanggaxiu	−0.965	2.035	0.105	0.98	−0.312	2.688	2.064	0.94
Lvcaogou upper layer	−0.999	2.001	0.003	0.97	−0.24	2.760	2.280	0.94
Lvcaogou lower layer	−0.766	2.234	0.702	0.99	−0.355	2.645	1.935	0.98

https://doi.org/10.1021/acsomega.4c00211
ACS Omega 2024, 9, 9823−9834

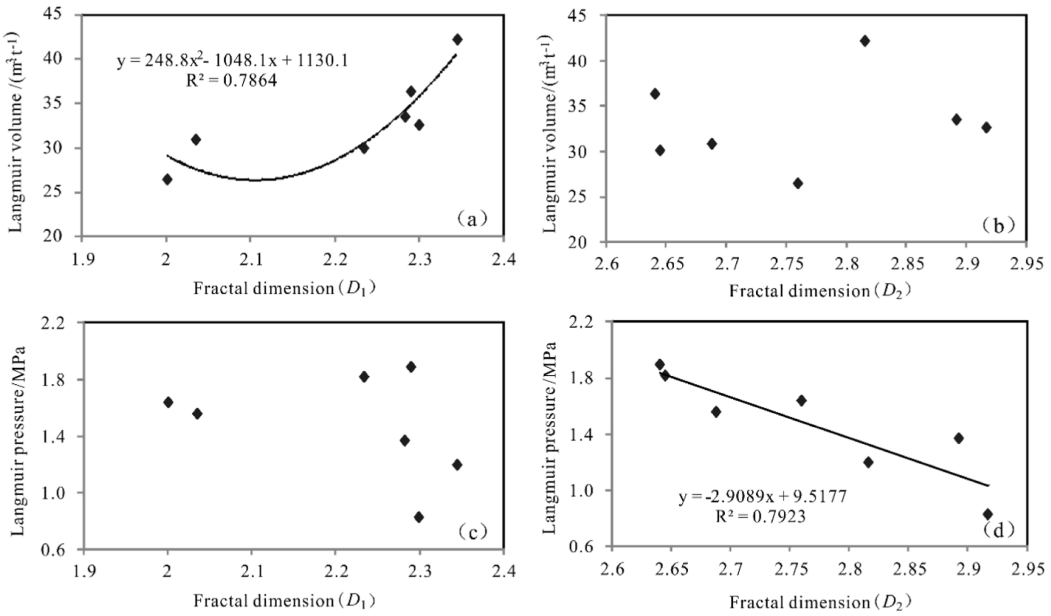

Figure 7. Relationship between Langmuir volume, Langmuir pressure, and fractal dimension. (a) Langmuir volume vs D_1; (b) Langmuir volume vs D_2; (c) Langmuir pressure vs D_1; (d) Langmuir pressure vs D_2.

be broken away. Therefore, this study adopts the calculation result of $A = D - 3$ and carries out the next step analysis.

According to the calculation results of fractal dimension, D_1 is relatively low, ranging from 2.001 to 2.345, and the distribution is relatively uniform, whereas D_2 is relatively high, ranging from 2.641 to 2.917, which decreases from west to east in the study area. This indicates that the structural complexity of the western study area is higher than that of the eastern area mainly due to the different influences of regional geological context. Specially, both orogenic belts, including Altun strike-slip fault and Qilian Mountain, affect the western area, whereas only Qilian Mountain affects the eastern area, resulting in more complex coal reservoirs and strata structural complexity.[38−40] The average D_2 of Saishiteng and Yuqia coalfields in the west is 2.88, and the mean D_2 of Quanji and Delingha coalfields in the east is 2.68. Compared with D_1 and D_2 data, it can be found that the fractal dimension D_1 has a little change and a high correlation coefficient, whereas the fractal dimension D_2 is significantly different, and the D_2 of type III with a weak hysteresis loop is significantly lower than that of type I and type II with an obvious hysteresis ring (Tables 1 and 2).

5.2. Relationship between Fractal Dimension of Adsorption Pore and CH_4 Adsorption Parameters. The fractal characterization of porous materials mainly includes the pore surface area and pore structure.[37] It is generally believed that when the hole surface shape dimension is equal to 2, it means that the coal surface is very smooth, and when it is equal to 3, it means that the coal surface is very rough. When the fractal dimension of the pore structure is equal to 2, the pore structure is very uniform, and when it is equal to 3, the pore structure is very complex, and the distribution of the pore throat is extremely uneven. For adsorption pores, D_1 represents the fractal dimension of the smaller adsorption pores in the coal sample. Because micropores are major contributors to the specific surface area of coal,[4] D_1 represents the fractal dimension of the surface area of adsorption pores. As mentioned above, D_2 represents the fractal dimension of the larger adsorption pores and is closely related to the strength of the hysteresis loop and thus represents different pore structure types.

The Langmuir volume represents the maximum adsorption capacity of coal samples, which is affected by a series of factors, including grain sizes, moisture, organic matter abundance, and pore structure, etc.[41−43] The influence of coal pore structure on adsorption capacity is the focus in this study. The fractal dimension D_1 reflects the micropore surface pore characteristics, and the fractal dimension D_1 shows a binomial correlation with Langmuir volume (Figure 7a). In general, Langmuir volume increases with the increase of fractal dimension D_1, but the relationship between fractal dimension D_2 and Langmuir volume of the coal sample is not obvious (Figure 7b). For Langmuir pressure, there is no obvious relationship with fractal dimension D_1 (Figure 7c), but there is a negative correlation with fractal dimension D_2 (Figure 7d). This is because the coals with large fractal dimension D_2 are not only complex in structure but also mostly have type I pores, which are characterized by absolute predominance of micropores and specific surface area. It indicates that the adsorption rate is higher in the low-pressure stage, corresponding to a larger adsorption amount, and there is an isothermal adsorption line with a larger curvature, thus the corresponding Langmuir pressure is lower (Figure 2c).

Therefore, both the fractal dimensions D_1 and D_2 have an impact on the methane adsorption parameters. Specifically, the coals with higher fractal dimension D_1 can provide more adsorption pore sites and have stronger methane adsorption capacity. The higher the fractal dimension D_2, the more complex the pore structure of coal. The stronger the pore heterogeneity, the lower the Langmuir pressure. Therefore, compared with primary coal, deformed coal tends to have a higher fractal dimension and a smaller average pore size.[44] In summary, coal samples with a higher pore surface fractal dimension and a lower pore structure fractal dimension not only have significantly enhanced methane adsorption capacity but can also effectively improve the desorption and diffusion rates of CBM.

https://doi.org/10.1021/acsomega.4c00211
ACS Omega 2024, 9, 9823−9834

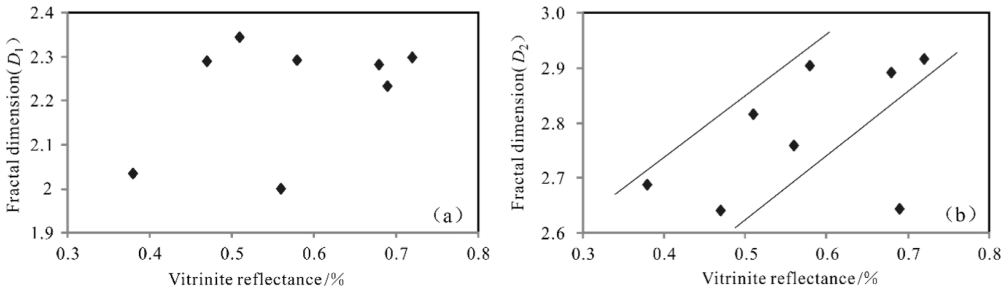

Figure 8. Relationship between vitrinite reflectance and fractal dimensions of coal samples. (a) D_1 vs vitrinite reflectance; (b) D_2 vs vitrinite reflectance.

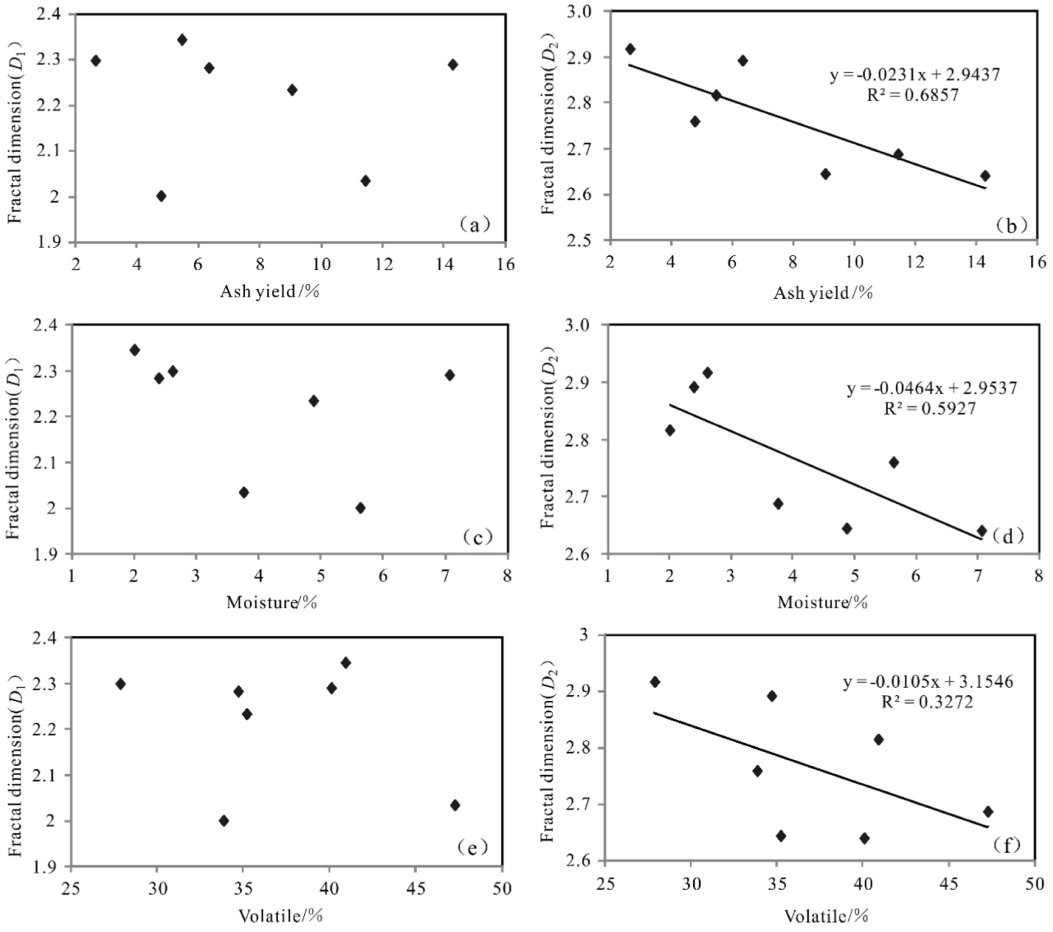

Figure 9. Relationships between ash yield, moisture content, volatile content, and fractal dimensions of coal samples. (a) D_1 vs ash yield; (b) D_2 vs ash yield; (c) D_1 vs moisture; (d) D_2 vs moisture; (e) D_1 vs volatile; (f) D_2 vs volatile.

5.3. Relationships between Fractal Dimension and Coal Material Composition and Pore Structure. *5.3.1. Relationship between Fractal Dimension and Coalification and Coal Quality Parameters.* Since the fractal dimension D_1 represents the surface fractal dimension of the adsorption pore, it has no obvious relationship with vitrinite reflectance of all coal samples (Figure 8a). Except for the sample of Lvcaogou lower layer, D_2 has a certain positive correlation with vitrinite reflectance (Figure 8b). When the coal metamorphism is low, different pore size volumes of adsorption pores are more uniform (such as Dameigou, Wanggaxiu, and Lvcaogou upper layers). With the increase of metamorphism, the volume of micropores increased significantly and pore throat distribution was not uniform, resulting in a more complex pore structure.

The relationships between the above two fractal dimensions and ash yield, moisture, and volatile matter are shown in Figure 10. The fractal dimension D_2 decreases with the increase of ash yield of coal because ash can fill some pores of the coal reservoir, making the pore structure relatively simple;[14] this results in a reduction in the fractal dimension D_2 (Figure 9b). Moisture and volatile components are the internal manifestations of the metamorphism of coal. With the increase in coalification, the dehydrogenation, deoxygenation, and carbon enrichment of organic compounds lead to the continuous reduction of side chains and functional groups on the corresponding polycondensates. The internal arrangement becomes more oriented and stable, and the fractal dimension D_2 gradually decreases (Figure 9d,f). In contrast, the fractal

https://doi.org/10.1021/acsomega.4c00211
ACS Omega 2024, 9, 9823−9834

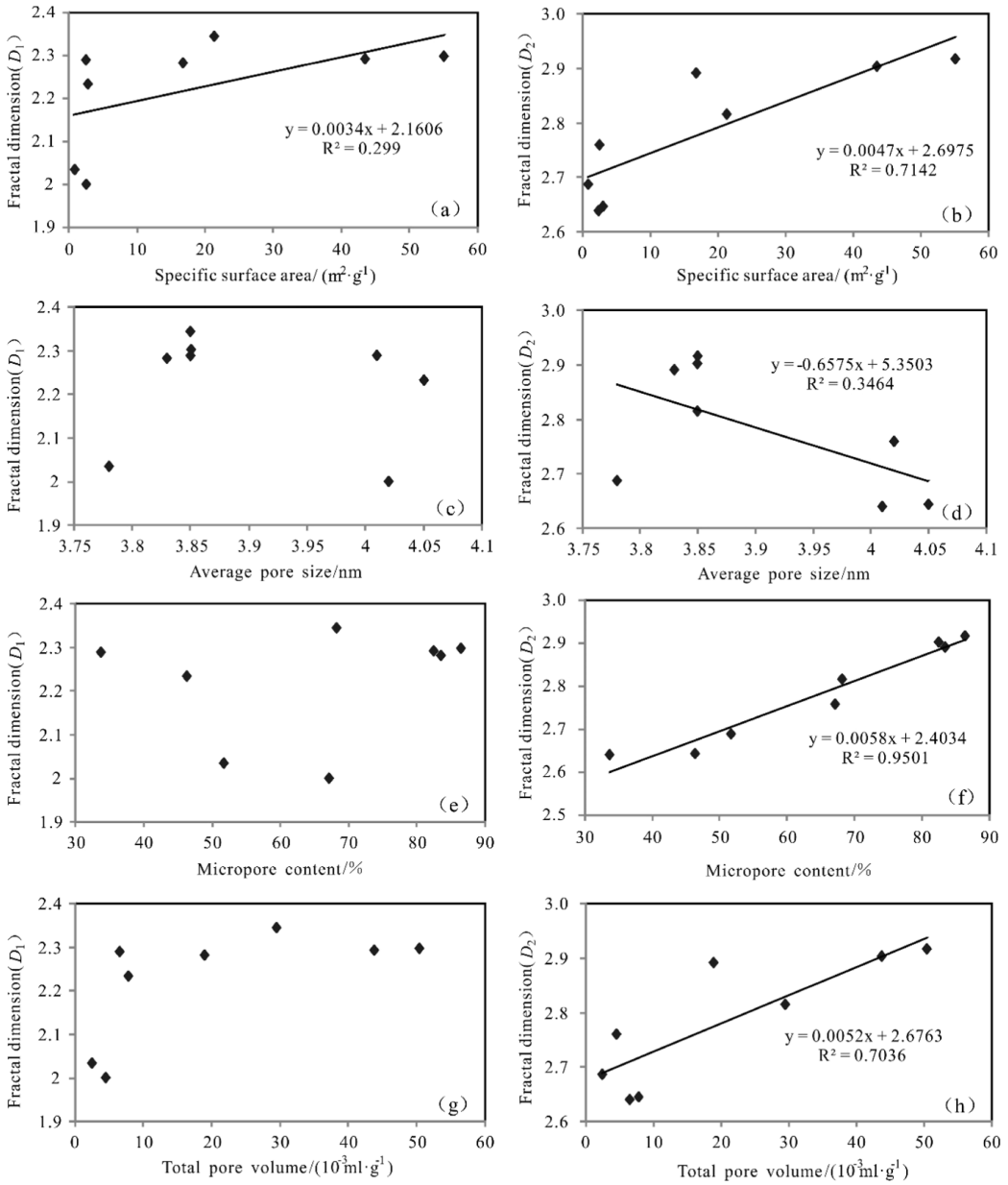

Figure 10. Relationships between specific surface area, average pore size, microporous content, total pore volume, and fractal dimensions. (a) D_1 vs specific surface area; (b) D_2 vs specific surface area; (c) D_1 vs average pore size; (d) D_2 vs average pore size; (e) D_1 vs micropore content; (f) D_2 vs micropore content; (g) D_1 vs total pore volume; (h) D_2 vs total pore volume.

dimension D_1 represents the surface fractal dimension of coal; thus, the relationship with ash yield, moisture, and volatiles of coal is not obvious (Figure 9a,c,e).

5.3.2. Relationships between Fractal Dimension and Coal Pore Structure. The fractal dimension D_1 is positively correlated with the specific surface area (Figure 10a), indicating that the coals with a higher specific surface area have a larger fractal dimension D_1, a greater specific surface area, and a stronger methane adsorption capacity (Figure 10a; Table 1). As the specific surface area of coal samples is positively correlated with the total pore volume (Figure 2a), the total pore volume increases with the increase of fractal dimension D_1 (Figure 10g). The fractal dimension D_2 is also positively correlated with the specific surface area. With the increase of micropore content (YQ-1 and Wucai coals), the heterogeneity of coal pores is enhanced due to the uneven distribution of various pores. Therefore, the fractal dimension D_2, representing the pore structure of coal, also increases accordingly (Figure 10b).

Since the fractal dimension D_1 represents the surface fractal dimension of adsorption pores, the relationships between D_1 and the average pore diameter and micropore content are not obvious (Figure 10c,e). However, the fractal dimension D_2 is negatively correlated with the average pore diameter (Figure 10d), indicating that the smaller the average pore diameter, the more complex the pore structure, which is also supported by other investigations.[45,46] Based on this phenomenon, we can infer that deformed coals with smaller pore sizes should correspond to a more complex pore structure compared with primary coals.[47] In addition, D_2 is positively correlated with the micropore volume percentage and total pore volume of coal samples, and the correlation coefficients (R^2) are 0.95 and

https://doi.org/10.1021/acsomega.4c00211
ACS Omega 2024, 9, 9823−9834

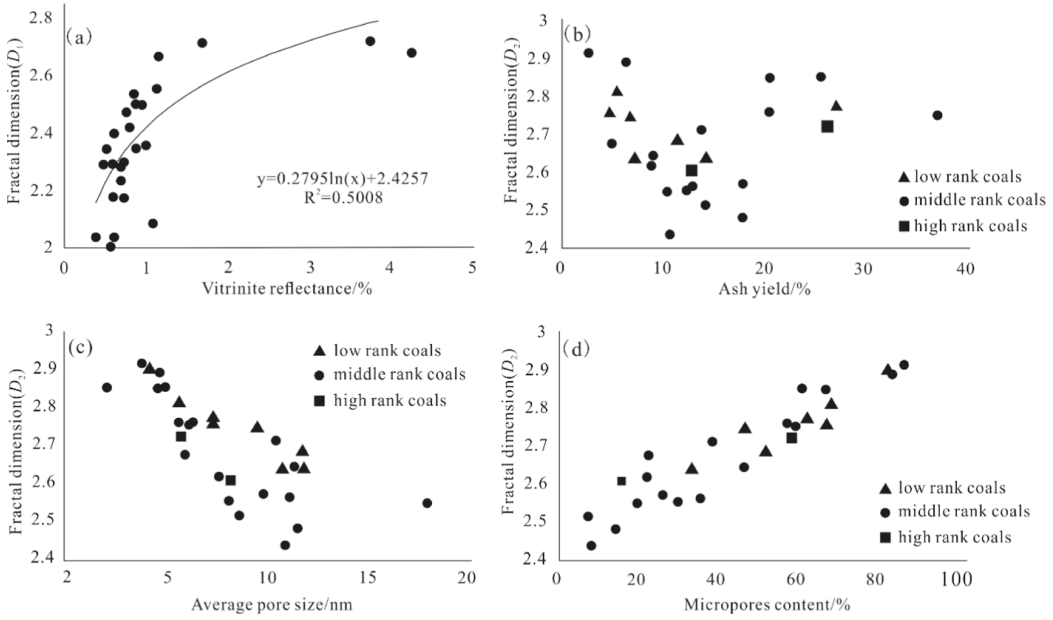

Figure 11. Relationships between maximum vitrinite reflectance, ash yield, average pore size, micropore content, and fractal dimensions (partial data derived from refs 13 and 51). (a) D_1 vs vitrinite reflectance; (b) D_2 vs ash yield; (c) D_2 vs average pore size; (d) D_2 vs micropores content.

0.70, respectively (Figure 10f,h), which indicates that the micropore content and total pore volume have a great influence on the pore structure and further confirms that the fractal dimension D_2 represents the pore structure characteristics of coal. The coal with a higher fractal dimension D_2 has a more complex pore structure.

5.4. Relationship between Fractal Dimension and Coal Parameters under Different Coalification Degrees. Generally, the fractal dimension of a coal pore is used to quantitatively characterize the complex pore structure, but indirect analysis of the fractal dimension and its physical significance based on the changes of various parameters in coals are rarely conducted. According to the analysis of the relationship between the fractal dimension of coal pores and the main coal parameters under different coal ranks, with the increase of vitrinite reflectance, the fractal dimension D_1 characterizing pore surface continues to rise (Figure 11a), indicating that the organic pore system in coals continues to develop and becomes gradually rough, thus the stronger methane adsorption capacity in coals can be found.[13] The relationship between ash yield in coal and fractal dimensions is not obvious (Figure 11b), indicating that the material composition of coal has no direct correlation with the development characteristics of the pore system, and it is more likely to be controlled by the depositional environment of peatland.[48] Under different coal rank conditions, the fractal dimension D_2 characterizing pore structure is negatively correlated with average pore size but positively correlated with micropore content (Figure 11c,d), indicating that the coal with a smaller average pore size and higher micropore content has a more complex pore structure. This can explain why deformed coals would have a more complex pore structure and a stronger methane adsorption capacity than those of primary coals.[47,48] To some degree, the vitrinite reflectance can be used to analyze the pore surface characteristics and methane adsorption capacity of coals. However, it should be noted that a majority of related data come from high-to-low volatile bituminous coals (Figure 11a), and the related data should be supported by brown coals and anthracite in the future. Also, the complexity of pore structure can be reflected according to the micropore content and average pore size of coals. Although coalification degree is the main factor influencing the variation of pore structure, other geological factors, such as coal macerals and structural conditions, also should be noted for one coalfield or basin.[49,50]

6. CONCLUSIONS

(1) Based on low-temperature nitrogen adsorption, the proportion of micropores is dominant in Jurassic low-ranked coals in northern Qaidam Basin. The specific surface area varies greatly, and it shows a positive linear correlation with total pore volume. The adsorption pore structure is divided into three types according to the nitrogen adsorption/desorption curve and pore size distribution.

(2) The fractal dimension D_1 of the adsorption pore surface is relatively low and evenly distributed, whereas the fractal dimension D_2 of the adsorption pore structure is relatively high and decreases from west to east, indicating that the pore structure of the western region in northern Qaidam Basin is more complex than that in the east.

(3) The fractal dimension D_1 has a good binomial correlation with the Langmuir volume of coal, whereas D_2 has a negative correlation with the Langmuir pressure. The fractal dimension D_1 is positively correlated with specific surface area and total pore volume, whereas the fractal dimension D_2 is positively correlated with coalification, specific surface area, micropore content, and total pore volume and negatively correlated with ash yield, moisture, volatile content, and average pore size.

(4) Based on the relationship between the fractal dimension and various coal parameters under different coalification grades, it can be found that the vitrinite reflectance can be used to analyze the pore surface characteristics and

https://doi.org/10.1021/acsomega.4c00211
ACS Omega 2024, 9, 9823−9834

methane adsorption capacity to some degree, and the complexity of coal pore structure can be reflected according to the micropore content and average pore size.

AUTHOR INFORMATION

Corresponding Author

Haihai Hou − *College of Mining, Liaoning Technical University, Fuxin 123000, China;* orcid.org/0000-0002-9891-979X; Email: houmensihai@163.com

Authors

Xuejiao Zhou − *College of Environmental Science and Engineering, Liaoning Technical University, Fuxin 123000, China*

Qian He − *College of Mining, Liaoning Technical University, Fuxin 123000, China*

Complete contact information is available at: https://pubs.acs.org/10.1021/acsomega.4c00211

Notes

The authors declare no competing financial interest.

ACKNOWLEDGMENTS

The coal sample collection received was great assistance from Baoming Guo from Lvcaogou coal mine and Lei Liu and Xuetian Wang from China University of Mining and Technology (Beijing). This study was also supported by the National Natural Science Foundation of China (42102223), the China Postdoctoral Science Foundation (2021M693844; 2022T150284), Open Fund for Key Laboratory of Green Development of Mineral Resources in Liaoning Province (LNTU/GDMR-2306), and Basic scientific research project of Liaoning Provincial Department of Education (LJKZ0369). The authors are also grateful for the careful and valuable comments from the anonymous reviewers.

REFERENCES

(1) Gan, H.; Nandi, S. P.; Walker, P. L. Nature of the porosity in American coals. *Fuel* **1972**, *51* (4), 272−277.

(2) Clarkson, C. R.; Bustin, R. M. The effect of pore structure and gas pressure upon the transport properties of coal: a laboratory and modeling study. 1. Isotherms and pore volume distributions. *Fuel* **1999**, *78* (11), 1333−1344.

(3) Chen, P.; Tang, X. The research on the adsorption of nitrogen in low temperature and micro-pore properties in coal. *J. China Coal Soc.* **2001**, *26* (5), 552−556.

(4) Zhong, L.-W.; Zhang, H.; Yuan, Z.-R.; et al. Influence of specific pore area and pore volume of coal on adsorption capacity. *Coal Geol. Explor.* **2002**, *30* (3), 26−29.

(5) Hodot, B. B. *Outburst of Coal and Coalbed Gas (Chinese Translation)*; China Industry Press: Beijing, 1966, pp 27−30.

(6) Shi, J.-Q.; Durucan, S. Gas storage and flow in coalbed reservoirs: Implementation of a bidisperse pore model for gas diffusion in a coal matrix. *SPE Reservoir Eval. Eng.* **2005**, *8* (02), 169−175.

(7) Hou, H. H. *Physical properties and comprehensive evaluation of coalbed methane reservoirs of Jurassic in the northern Qaidam Basin*; China University of China Mining and Technology: Beijing, 2015, pp 39−41.

(8) Liu, H. L.; Wang, H. Y.; Zhao, Q.; et al. Geological characteristics of coalbed methane and controlling factors of accumulation in the Tuha Coal Basin. *Acta Geol. Sin.* **2010**, *84* (1), 133−136.

(9) Hou, H.-H.; Shao, L.-Y.; Tang, Y.; et al. Criteria for selected areas evaluation of low rank CBM based on multi-layered fuzzy mathematics: A case study of Turpan-Hami Basin. *Geol. China* **2014**, *41* (3), 1002−1009.

(10) Li, S.; Mao, X. P.; Tang, D. Z.; et al. Resource assessment of coal-derived gas in Huhehu depression, Hailar Basin. *Geol. China* **2009**, *36* (6), 1350−1358.

(11) Hazra, B.; Wood, D. A.; Vishal, V.; Singh, A. K. Pore characteristics of distinct thermally mature shales: Influence of particle size on low-pressure CO_2 and N_2 adsorption. *Energy Fuels* **2018**, *32* (8), 8175−8186.

(12) Song, X.-X.; Tang, Y.-G.; Li, W.; et al. Fractal characteristics of adsorption pores of tectonic coal from Zhongliangshan southern coalmine. *J. China Coal Soc.* **2013**, *38* (1), 134−139.

(13) Yao, Y.; Liu, D.; Tang, D.; Tang, S.; Huang, W. Fractal characterization of adsorption-pores of coals from North China: An investigation on CH_4 adsorption capacity of coals. *Int. J. Coal Geol.* **2008**, *73* (1), 27−42.

(14) Zhang, S.-H.; Tang, S.-H.; Tang, D.-Z.; et al. Fractal characteristics of coal reservoir seepage pore, east margin of Ordos Basin. *J. China Univ. Min. Technol.* **2009**, *5* (38), 713−718.

(15) Pan, J.; Du, X.; Wang, X.; Hou, Q.; Wang, Z.; Yi, J.; Li, M. Pore and permeability changes in coal reservoirs induced by true triaxial $ScCO_2$ fracturing based on low-field nuclear magnetic resonance. *Energy* **2024**, *286*, 129492.

(16) Pan, J.; He, H.; Li, G.; Wang, X.; Hou, Q.; Liu, L.; Cheng, N. Anisotropic strain of anthracite induced by different phase CO_2 injection and its effect on permeability. *Energy* **2023**, *284*, 128619.

(17) Wang, X.; Pan, J.; Wang, K.; Mou, P.; Li, J. Fracture variation in high-rank coal induced by hydraulic fracturing using X-ray computer tomography and digital volume correlation. *Int. J. Coal Geol.* **2022**, *252*, 103942.

(18) Hou, H.; Qin, Q.; Shao, L.; Liang, G.; Tang, Y.; Zhang, H.; Li, Q.; Liu, S. Study on the applicability of reservoir fractal characterization in middle-high rank coals with NMR: Implications for pore-fracture structure evolution within the coalification process. *ACS Omega* **2021**, *6* (48), 32495−32507.

(19) Yu, E. X.; Ma, L. T.; Zhou, F. H.; et al. Study on method to characterize fractal features of pore structures in coal and rock mass. *Coal Sci. Technol.* **2018**, *46* (11), 8−12.

(20) Liu, S. Q.; Wang, H.; Wang, R.; et al. Research advances on characteristics of pores and fractures in coal seams. *Acta Sedimentol. Sin.* **2021**, *39* (01), 212−230.

(21) Kuila, U.; Prasad, M. Specific surface area and pore-size distribution in clays and shales. *Geophys. Prospect.* **2013**, *61*, 341−362.

(22) Singh, D. P.; Chandra, D.; Vishal, V.; Hazra, B.; Sarkar, P. Impact of degassing time and temperature on the estimation of pore attributes in shale. *Energy Fuels* **2021**, *35* (19), 15628−15641.

(23) Meng, J.; Wang, L.; Wang, J.; Zhang, S. Characterization and analysis of molecular-scale pore structure of coal with different metamorphic degrees. *Energy Fuels* **2023**, *37* (5), 3634−3653.

(24) Peter, C.; Borello, E. S.; Baietto, O.; Bellopede, R.; Panini, F.; Massimiani, A.; Marini, P.; Viberti, D. Quantitative characterization of marble natural aging through pore structure image analysis. *J. Mater. Civ. Eng.* **2023**, *35* (9), 15161.

(25) Liu, T. J.; Shao, L. Y.; Cao, D. Y.; et al. *Formation conditions and evaluation of coal resources of the Middle Jurassic in the northern Qaidam Basin*; Geological Publishing House: Beijing, 2013, pp 249−268.

(26) Li, M.; Shao, L.; Lu, J.; Spiro, B.; Wen, H.; Li, Y. Sequence stratigraphy and paleogeography of the Middle Jurassic coal measures in the Yuqia Coalfield, northern Qaidam Basin, northwestern China. *AAPG Bull.* **2014**, *98* (12), 2531−2550.

(27) Hou, H.; Shao, L.; Li, Y.; Liu, L.; Liang, G.; Zhang, W.; Wang, X.; Wang, W. Effect of paleoclimate and paleoenvironment on organic matter accumulation in lacustrine shale: Constraints from lithofacies and element geochemistry in the northern Qaidam Basin, NW China. *J. Pet. Sci. Eng.* **2022**, *208*, 109350.

(28) Sethi, C.; Mastalerz, M.; Hower, J. C.; Hazra, B.; Singh, A. K.; Vishal, V. Using optical-electron correlative microscopy for shales of contrasting thermal maturity. *Int. J. Coal Geol.* **2023**, *274*, 104273.
(29) Bustin, R. M.; Clarkson, C. R. Geological controls on coalbed methane reservoir capacity and gas content. *Int. J. Coal Geol.* **1998**, *38* (1−2), 3−26.
(30) Sang, S.-X.; Qin, Y.; Guo, X.-B.; et al. Storing characteristics of Jurassic coalbed gas in Junggar and Tuha Basins. *Geol. J. China Univ.* **2003**, *9* (3), 365−368.
(31) Yao, Y. B.; Liu, D. M. *Advanced quantitative characterization and comprehensive evaluation model of coalbed methane reservoirs*; Geological Publishing House: Beijing, 2013, pp 33−34.
(32) Hazra, B.; Wood, D. A.; Vishal, V.; Varma, A. K.; Sakha, D.; Singh, A. K. Porosity controls and fractal disposition of organic-rich Permian shales using low-pressure adsorption techniques. *Fuel* **2018**, *220*, 837−848.
(33) Tang, S.-H.; Zhang, J.-P.; Wu, M.-J. The pore structure characteristics about the sapropelic coal. *Nat. Gas Geosci.* **2013**, *24* (2), 247−251.
(34) Li, Z.; Ren, T.; Li, X.; Qiao, M.; Yang, X.; Tan, L.; Nie, B. Multi-scale pore fractal characteristics of differently ranked coal and its impact on gas adsorption. *Int. J. Min. Sci. Technol.* **2023**, *33* (4), 389−401.
(35) Zhou, X.; Hou, H.; Li, H. Influence of coalification on pore structure evolution in middle-ranked coals. *Front. Earth Sci.* **2023**, *11*, 1139852.
(36) Qi, H.; Ma, J.; Wong, P.-Z. Adsorption isotherms of fractal surfaces. *Colloids Surf., A* **2002**, *206* (1−3), 401−407.
(37) Pyun, S. I.; Rhee, C. K. An investigation of fractal characteristics of mesoporous carbon electrodes with various pore structures. *Electrochim. Acta* **2004**, *49* (24), 4171−4180.
(38) Hou, H.; Liu, S.; Shao, L.; Li, Y.; Zhao, M.; Wang, C. Elemental geochemistry of the Middle Jurassic shales in the northern Qaidam Basin, northwestern China: Constraints for tectonics and paleoclimate. *Open Geosci.* **2021**, *13*, 1448−1462.
(39) Jiang, L.; Liu, Y.; Li, W.; Yuan, S.; Yuan, J.; Li, S.; Liu, Z. Cenozoic double-layered structure in the western Qaidam Basin, northern Tibetan Plateau, China. *J. Asian Earth Sci.* **2022**, *232*, 105123.
(40) Hu, X.; Wu, L.; Zhang, Y.; Zhang, J.; Wang, C.; Tang, J.; Xiao, A.; Chen, H.; Yang, S. Multiscale lithospheric buckling dominates the Cenozoic subsidence and deformation of the Qaidam Basin: A new model for the growth of the northern Tibetan Plateau. *Earth-Sci. Rev.* **2022**, *234*, 104201.
(41) Varma, A. K.; Biswal, S.; Hazra, B.; Mendhe, V. A.; Misra, S.; Samad, S. K.; Singh, B. D.; Dayal, A. M.; Mani, D. Petrographic characteristics and methane sorption dynamics of coal and shaly-coal samples from Ib Valley Basin, Odisha, India. *Int. J. Coal Geol.* **2015**, *141−142*, 51−62.
(42) Laxminarayana, C.; Crosdale, P. J. Role of coal type and rank on methane sorption characteristics of Bowen Basin, Australia coals. *Int. J. Coal Geol.* **1999**, *40* (4), 309−325.
(43) Crosdale, P. J.; Moore, T. A.; Mares, T. E. Influence of moisture content and temperature on methane adsorption isotherm analysis for coals from a low-rank, biogenically-sourced gas reservoir. *Int. J. Coal Geol.* **2008**, *76* (1−2), 166−174.
(44) Gao, B.; Huang, H. Z.; Ning, N.; et al. Pore size characteristics of tectonic coal and its influence on gas bearing properties. *Coal Geol. Explor.* **2018**, *46* (5), 182−187.
(45) Hou, H.; Shao, L.; Tang, Y.; Zhao, S.; Yuan, Y.; Li, Y.; Mu, G.; Zhou, Y.; Liang, G.; Zhang, J. Quantitative characterization of low-rank coal reservoirs in the southern Junggar Basin, NW China: Implications for pore structure evolution around the first coalification jump. *Mar. Pet. Geol.* **2020**, *113*, 104165.
(46) Chen, X.; Ma, R.; Wu, J.; Sun, J. Fractal analysis of coal pore structure based on computed tomography and fluid intrusions. *Fractal Fract.* **2023**, *7* (6), 439.
(47) Zhang, K.; Liu, H.; Ma, M.; Xu, H.; Fang, H. Multiscale Fractal characterization of pore-fracture structure of tectonically deformed coal compared to primary undeformed coal: Implications for CO_2 geological sequestration in coal seams. *Processes* **2023**, *11* (10), 2934.
(48) Hou, H.; Shao, L.; Tang, Y.; Li, Z.; Zhao, S.; Yao, M.; Wang, X.; Zhang, J. Pore structure characterization of middle- and high-ranked coal reservoirs in northern China. *AAPG Bull.* **2023**, *107* (2), 213−241.
(49) Misz-Kennan, M.; Kus, J.; Flores, D.; Avila, C.; Büçkün, Z.; Choudhury, N.; Christanis, K.; Joubert, J. P.; Kalaitzidis, S.; Karayigit, A. I.; et al. Development of a petrographic classification system for organic particles affected by self-heating in coal waste. (An ICCP Classification System, Self-heating Working Group - Commission III). *Int. J. Coal Geol.* **2020**, *220*, 103411.
(50) Li, S.; Qin, Y.; Tang, D.; Shen, J.; Wang, J.; Chen, S. A comprehensive review of deep coalbed methane and recent developments in China. *Int. J. Coal Geol.* **2023**, *279*, 104369.
(51) Yao, M. L.; Shao, L. Y.; Hou, H. H.; et al. Coal reservoir adsorptive pore structural and fractal features in Huainan and Huaibei Coalfields. *Coal Geol. China* **2018**, *30* (1), 30−36.

https://doi.org/10.1021/acsomega.4c00211
ACS Omega 2024, 9, 9823−9834